Nuclear Instruments and Methods in Physics Research B 269 (2011) 1208–1211

Contents lists available at ScienceDirect

Nuclear Instruments and Methods in Physics Research B

journal homepage: www.elsevier.com/locate/nimb

Fast atom diffraction for grazing scattering of Ne atoms from a LiF(001) surface

M.S. Gravielle [a,b,*], A. Schüller [c], H. Winter [c], J.E. Miraglia [a,b]

[a] Instituto de Astronomía y Física del Espacio (CONICET-UBA), Casilla de correo 67, sucursal 28 (C1428EGA), Buenos Aires, Argentina
[b] Departamento de Física, Fac. de Ciencias Exactas y Naturales, Universidad de Buenos Aires, Argentina
[c] Institut für Physik, Humboldt Universität zu Berlin, Newtonstrasse 15, D-12489 Berlin-Adlershof, Germany

ARTICLE INFO

Article history:
Received 22 September 2010
Received in revised form 28 November 2010
Available online 9 December 2010

Keywords:
Diffraction
Atom
Surface
Collision

ABSTRACT

Angular distributions of fast Ne atoms after grazing collisions with a LiF(001) surface under axial surface channeling conditions are experimentally and theoretically studied. We use the surface eikonal approximation to describe the quantum interference of scattered projectiles, while the atom–surface interaction is represented by means of a pairwise additive potential, including the polarization of the projectile atom. Experimental data serve as a benchmark to investigate the performance of the proposed potential model, analyzing the role played by the projectile polarization.

1. Introduction

Diffraction of swift atoms, with energies in the keV range, during grazing scattering from crystal surfaces [1,2] has attracted remarkable attention [3–9] . In particular, due to the high sensitivity to the projectile–surface interaction [3,5–7,10], fast atom diffraction is a powerful tool to probe surface potentials, opening the way for the development of an accurate surface analytical technique [11,12].

Until now, most of the research on this diffraction phenomenon was carried out using light atoms, like H or He, as projectiles. In this article we study experimentally and theoretically axial surface channeling of a heavier projectile – neon – for which interference effects have been also reported [3]. Here, as a continuation of previous works [3,13] on the Ne–LiF(001) system, we analyze the angular positions of diffraction peaks quantitatively. Our goal is to use diffraction patterns in order to test the validity of pairwise additive potentials [14] for an atom with several electrons interacting with an ionic crystal surface. The Ne–LiF surface interaction is represented as a sum of individual interatomic potentials, which takes into account contributions from the different ionic centers of the insulator material, including the projectile polarization. This approach is simplified with respect to interaction potentials obtained from ab initio calculations, which are complex, time consuming, and may be unreliable at the small energies [15] relevant here. For the interaction of noble gas atoms as Ne and closed shell ions as Li^+ and F^- ions of the LiF(001) surface, the superposition of binary interatomic potentials is a good approximation for the description of classical scattering at grazing incidence [13]. In this work we show that even at small energies, in the regime where diffraction effects for fast atoms are present, the approximation of the surface by free and unperturbed ions is adequate if attractive contributions due to the polarization of the noble gas atom are taken into account.

To describe the scattering process we employ a distorted-wave model – the surface eikonal approximation [5] – that makes use of the eikonal wave function to represent the elastic collision with the surface. On the other hand, the motion of the fast projectile is classically described by considering axially channeled trajectories for different initial conditions. This method is a semi-classical approximation that includes a clear description of the main mechanisms of the process, being simpler to be used than a full quantum calculation in terms of a wave packet propagation [2,6]. The surface-eikonal approximation has been successfully applied to investigate fast atom diffraction of helium atoms scattered from insulator surfaces [10,16]. In comparison to other approaches [3,6], the corrugation of the complete three dimensional surface plane was taken into account without averaging the projectile–surface potential along the incidence direction.

By comparing eikonal angular spectra with experimental angular distributions for different incidence energies and channels we are able to determine the range of applicability for our potential model. As also observed for He projectiles [5,10], we find that the projectile polarization is important for impact along the ⟨110⟩ channel but plays a minor role for incidence in the ⟨100⟩ direction.

* Corresponding author at: Instituto de Astronomía y Física del Espacio (CONICET-UBA), Casilla de correo 67, sucursal 28 (C1428EGA), Buenos Aires, Argentina. Tel.: +54 11 4781 6755; fax: +54 11 4786 8114.
E-mail address: msilvia@iafe.uba.ar (M.S. Gravielle).

0168-583X/$ - see front matter © 2010 Elsevier B.V. All rights reserved.
doi:10.1016/j.nimb.2010.12.011

The experimental method and the theoretical formalism are summarized in Sections 2 and 3, respectively. Results are presented and discussed in Section 4, and in Section 5 we outline our conclusions. Atomic units ($e^2 = \hbar = m_e = 1$) are used unless otherwise stated.

2. Experimental method

In our experiments we have scattered neutral Ne atoms with kinetic energies E_i ranging from 0.8 keV to 25 keV from a clean and flat LiF(001) surface at room temperature under grazing angles of incidence $0.4 < \Phi_{in} < 2^\circ$. Fast Ne^+ ion beams were produced in a 10 GHz electron cyclotron resonance (ECR) ion source (Nanogan Pantechnique, Caen, France). The neutralization of the Ne^+ ions was achieved via charge transfer in a gas cell mounted in the beam line of the accelerator operating with Ne gas and subsequent deflection of remaining ions by an electric field. A base pressure of some 10^{-11} mbar was achieved in our UHV chamber by a turbomolecular pump in series with a titanium sublimation pump, where the pressure gradient with respect to the beam line of the accelerator was maintained by two differential pumping stages. Pairs of slits at both ends of these stages were used for the collimation of the incident beam to a divergence of <0.03°. This high collimation is needed in order to achieve a sufficient degree of coherence for the scattering process.

The LiF(001) surface was prepared by cycles of grazing sputtering with 25 keV Ar^+ ions at 250 °C where the ionic conductivity of LiF is sufficiently enhanced in order to avoid macroscopic charging up and subsequent annealing to temperatures of about 350 °C. The scattering experiments were performed in the regime of axial surface channeling, i.e. the azimuthal setting of the surface plane was chosen such that the direction of the incident beam was parallel with atomic strings along low indexed directions in the surface plane.

2D angular distributions of scattered projectiles were recorded by means of a commercially available position-sensitive multichannelplate detector (MCP) with a delay-line anode (DLD40, Roentdek Handels GmbH) located 66 cm behind the target. This provides a simple and very efficient procedure for recording data, where complete diffraction patterns, as shown below, can be recorded in a time of typically minutes. Since only about 10^4 projectiles per second hit the target surface, fast atom diffraction is non-destructive and can be applied in studies on insulator surfaces (neutral projectiles) [1,2], as well as adsorption phenomena at metal surfaces [7,12]. Recent work has demonstrated fast atom diffraction also for clean metal surfaces [4,8,17], semiconductor [11,18] surfaces, and thin films on metal substrates [19].

3. Theoretical model

Within the surface eikonal model the transition matrix per unit area $\mathcal{A}$ reads [5]

$$T_{if}^{(eik)} = \frac{1}{\mathcal{A}} \int_{\mathcal{A}} d\vec{R}_{os}\, a_{if}(\vec{R}_{os}), \tag{1}$$

where $\vec{R}_{os}$ determines the initial position of the projectile on the surface plane and

$$a_{if}(\vec{R}_{os}) = \frac{1}{(2\pi)^3} \int_{-\infty}^{+\infty} dt \left| v_z(\vec{\mathcal{R}}_P) \right| \times \exp[-i\vec{Q}\cdot\vec{\mathcal{R}}_P - i\eta(\vec{\mathcal{R}}_P)] V_{SP}(\vec{\mathcal{R}}_P) \tag{2}$$

is the transition amplitude associated with the classical path $\vec{\mathcal{R}}_P(\vec{R}_{os}, t)$, with $v_z(\vec{\mathcal{R}}_P)$ being the component of the projectile velocity perpendicular to the surface plane. In Eq. (2) $\vec{Q} = \vec{K}_f - \vec{K}_i$ denotes the projectile momentum transfer, with $\vec{K}_{i(f)}$ the initial (final) projectile momentum satisfying the energy conservation, i.e. $K_f = K_i$. The phase η is the eikonal-Maslov phase, which is defined along the projectile path as [16]

$$\eta(\vec{\mathcal{R}}_P) = \int_{-\infty}^{t} dt'\, V_{SP}(\vec{\mathcal{R}}_P(t')) + \phi_M, \tag{3}$$

where V_{SP} is the projectile–surface interaction and $\phi_M = \nu\pi/2$ is the Maslov correction term, with ν the Maslov index as defined in Ref. [20]. Note that the surface eikonal approach takes into account the quantum interference between different axially channeled projectile trajectories. The basic idea is similar to the one of the semiclassical formalism applied in Ref. [3]. But in contrast to such an approximation, which is derived using classical cross sections, the surface eikonal model is based on a quantum formalism which involves the coherent addition of complex transition amplitudes.

A key quantity within the surface eikonal approximation is the potential V_{SP}, which determines not only the eikonal phase but also the classical projectile trajectories. In this work the projectile–surface potential is expressed by the sum of the static and polarization contributions, i.e. $V_{SP} = V_{SP}^{(st)} + V_{SP}^{(pol)}$. The static potential, $V_{SP}^{(st)}$, represents the interaction between the atom and the crystal surface derived by assuming that their electronic densities remain frozen when the atom approaches the surface. This term is described by adding individual contributions corresponding to the different solid ions (pairwise hypothesis). As we are dealing with an ionic insulator, where all electrons are strongly localized around the ionic nucleus, and Ne is a close-shell atom, the pairwise additive hypothesis is expected to be a reliable approach [21]. For the calculation of $V_{SP}^{(st)}$, each of the binary projectile – solid ion potentials was obtained from the Abrahamson model [22], which is equivalent to the one employed by Kim and Gordon [23]. The polarization potential $V_{SP}^{(pol)}$ originates from the rearrangement of the projectile electron density induced by the presence of target ions. It is given by

$$V_{SP}^{(pol)}(\vec{R}) = -\frac{\alpha}{2} \left| \sum_i \frac{Z_{Ti}^{(eff)}(R_i)}{R_i^2} \widehat{R}_i \right|^2, \tag{4}$$

where α is the atomic polarizability, with $\alpha = 2.67$ a.u. for neon [24], and the sum formally includes all ions of the target crystal, with $\vec{R}_i$ the position vector of the projectile with respect to the target ion labelled as i and $\widehat{R}_i = \vec{R}_i/R_i$. In order to make each term of Eq. (4) finite at the origin, we have introduced an effective charge for the target ion i, defined as $Z_{Ti}^{(eff)}(R_i) = Z_{Ti}^{(\infty)}[1 - (1 + \tilde{r}_i + \tilde{r}_i^2/2)\exp(-\tilde{r}_i)]$, where $\tilde{r}_i = R_i/R_{0i}$, R_{0i} is a screening parameter, determined by the target and projectile mean radii [25], and $Z_{Ti}^{(\infty)}$ is the asymptotic ionic charge, with $Z_{Ti}^{(\infty)} = 1$ and -1 for Li^+ and F^-, respectively. Note that $Z_{Ti}^{(eff)}(R_i)$ provides the proper limit of the polarization potential at intermediate distances, in contrast to the previously used Buckingham screening [5,10] which includes incorrect R_i^{-6} terms [26]. In the evaluation of the static and polarization contributions we have considered a surface rumpling derived from an ab initio calculation reported in Ref. [16]. However, for Ne projectiles the neglect of the surface rumpling hardly changes the calculated distributions. Details of the calculation are given in Refs. [5,10].

4. Results

In Fig. 1(a) we show the experimental distribution of Ne^0 atoms elastically scattered from a LiF(001) surface after grazing incidence along the ⟨110⟩ direction, as function of the angles Φ_{out} and Ψ. These angles correspond to the polar and azimuthal exit angles, respectively, of the projectiles, with Ψ measured with respect to the incidence direction in the surface plane. As observed for light atoms, the angular distribution in Fig. 1(a) shows maxima

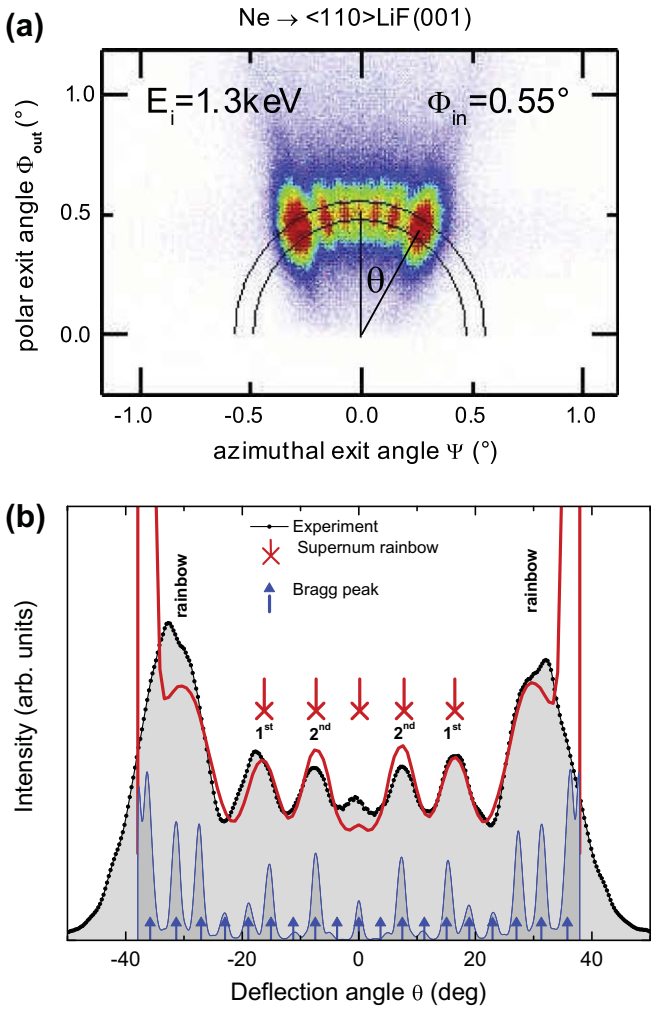

Fig. 1. (a) Two dimensional intensity distribution, as recorded with a position sensitive detector, for Ne atoms scattered from LiF(001) along the ⟨110⟩ channel. The incidence energy and angle are $E_i = 1.3$ keV and $\Phi_{in} = 0.55°$, respectively. Color code: Red = high, blue = low intensity. (b) Projected intensity inside the annulus from Fig. 1(a), as a function of the deflection angle θ (gray circles) and corresponding differential probabilities derived from the surface eikonal approach, considering $n_\perp = 1$ (red solid line) and $n_\perp = 3$ (blue dashed line) reduced unit cells, as explained in the text [30]. (For interpretation of the references to colour in this figure legend, the reader is referred to the web version of this article.)

symmetrically placed with respect to $\Psi = 0$, inside an annulus of radius Φ_{in}, with the incidence angle Φ_{in} measured with respect to the surface plane. In order to study the intensity profile in detail, the experimental intensity inside the annulus from Fig. 1(a) is displayed in Fig. 1(b) as function of the deflection angle θ, defined as $\theta = \arctan(\Psi/\Phi_{out})$. The outermost peaks of the distribution shown in Fig. 1(b) are associated with rainbow scattering, having a classical origin, while the inner peaks are related to supernumerary rainbows, stemming from quantum interference effects. Similar structures are also displayed by the eikonal spectrum obtained from Eq. (1) considering the integration area $\mathcal{A}$ as *one* reduced unit cell. The positions of the supernumerary rainbows are well reproduced by the eikonal angular distribution, being indicative of the quality of the proposed potential model. Note that at the extreme angles the eikonal spectrum shows sharp maxima, not present in the experiment. These peaks at classical rainbow angles originate from the semiclassical description of the projectile motion, which does not include the finite intensity on the dark side of the classical rainbow [27]. However, this deficiency of the eikonal approach does not affect supernumerary rainbows at smaller deflection angles.

As discussed in Refs. [3,9,16], diffraction patterns have two different origins: supernumerary rainbows and Bragg diffraction. Both mechanisms are included in the eikonal description and can be analyzed separately as follows. In Eq. (1) the integration region on the surface plane, $\mathcal{A}$, is in principle determined by the size of the initial wave packet of incident projectiles [28]. By considering this area as composed by n identical reduced unit cell, each of them centered on a different site $\vec{X}_{sj}$ of the crystal surface, we can express the corresponding eikonal transition matrix as

$$T_{if,n}^{(eik)} = T_{if,1}^{(eik)} S_n(\vec{Q}_s), \tag{5}$$

where $T_{if,1}^{(eik)}$ is derived from Eq. (1) by evaluating the $\vec{R}_{os}$-integral over *one* reduced unit cell, while the function

$$S_n(\vec{Q}_s) = \frac{1}{n}\sum_{j=1}^{n} \exp\left[-i\vec{Q}_s \cdot \vec{X}_{sj}\right] \tag{6}$$

takes into account the crystallographic structure of the surface, with $\vec{Q}_s$ the momentum transfer parallel to the surface plane. Each factor in Eq. (5) describes a different mechanism. The factor $T_{if,1}^{(eik)}$ is related to supernumerary rainbows and carries information on the shape of the interaction potential across the incidence channel, being produced by the interference of trajectories whose initial positions $\vec{R}_{os}$ differ by a distance smaller than d, with d being the spatial lattice periodicity of the channel. The factor $S_n(\vec{Q}_s)$ is associated with the Bragg diffraction and provides information on the spacing between surface atoms only. As the component of the momentum transfer along the incidence channel is negligible, we can approximate $S_n(\vec{Q}_s) \approx S_n(Q_{s\perp})$, where $Q_{s\perp} = K_f \cos\Phi_{out} \sin\Psi$is the component of the parallel transferred momentum perpendicular to the incidence channel. For scattering along the ⟨110⟩ channel this function reads $S_n(Q_{s\perp}) = \sin(n_\perp\beta)/(n_\perp \sin\beta)$, with $n_\perp$ being the number of reduced unit cells along the perpendicular direction and $\beta = Q_{s\perp}d/2$. Hence, $S_n(\vec{Q}_s)$ gives rise to Bragg maxima placed at $Q_{s\perp}d = m2\pi$, with m an integer number, the width of such peaks being affected by the number of reduced unit cells reached by the incident wave packet, i.e. the larger $n_\perp$ is, the narrower the Bragg peaks are. In Fig. 1(b) we also display the eikonal spectrum obtained from Eq. (1) by considering *three* reduced unit cells, which presents Bragg maxima as superimposed structures to the supernumerary contribution. Discrete Bragg peaks originated from the interference of trajectories from different reduced unit cells as for light atoms [16] are not present in the experimental distribution due to the limits in spatial resolution of the detector. Furthermore, the coherence for diffraction in terms of Bragg peaks might be destroyed as a result of decoherence processes, as e.g. the influence of the thermal vibrations of the surface atoms [29]. The supernumerary rainbows, however, are more robust against decoherence [9]. Then, we neglect the Bragg peaks in the simulation by taking into account one reduced unit cell only.

With the incidence energy $E_i = E_{i\parallel} + E_{i\perp}$, where $E_{i\parallel} = E_i \cos^2\Phi_{in}$ and $E_{i\perp} = E_i \sin^2\Phi_{in}$ are associated to the initial motion parallel and perpendicular to the axial channel, we observe that the spectra as a function of the deflection angle θ are mainly determined by $E_{i\perp}$. That is, position and number of the supernumerary maxima are independent of E_i for the same $E_{i\perp}$ [16]. Then, since different perpendicular energies $E_{i\perp}$ probe a different z-range of V_{SP}, in Fig. 2 we plot the angular positions of the maxima of the experimental distribution as a function of $E_{i\perp}$ in order to investigate the atom–surface potential across the ⟨110⟩ channel in the range from 0.07 to 0.5 eV. Note that for Ne projectiles, as a consequence of its large mass, the energy range where supernumerary maxima can experimentally be resolved is smaller than for helium impact. The surface eikonal approximation using a pairwise additive

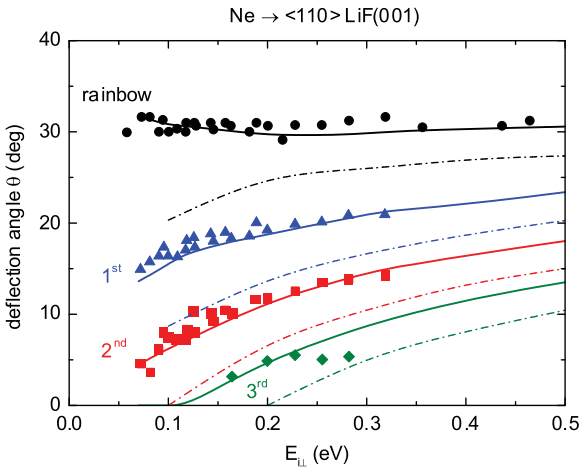

Fig. 2. Deflection angles θ corresponding to maxima of angular distributions, as a function of the perpendicular energy $E_{i\perp}$, for Ne atoms scattered from LiF(001) along the $\langle 110 \rangle$ direction. Symbols: experimental data for rainbow (circles) and first (triangles), second (squares), and third (diamonds) supernumerary rainbow angles. Curves: eikonal calculation of quantum rainbow and supernumerary rainbows derived with a pairwise additive potential, including (solid) and without including (dot-dashed) polarization.

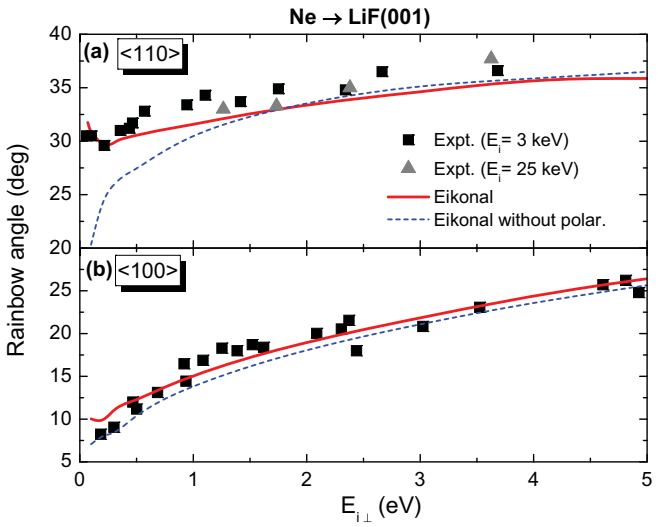

Fig. 3. Rainbow angle, as function of the perpendicular energy $E_{i\perp}$, for Ne atoms scattered from LiF(001) along the directions (a) $\langle 110 \rangle$ and (b) $\langle 100 \rangle$. Symbols: experimental data. Curves: quantum rainbow derived within the surface eikonal approximation, including (red full) and without including (blue dashed) polarization. (For interpretation of the references to colour in this figure legend, the reader is referred to the web version of this article.)

potential reproduces fairly well positions of rainbow and supernumerary rainbow maxima over the whole energy range. This represents a sensitive test for the corrugation of the potential across the channel. When the polarization contribution is neglected, the eikonal curves largely underestimate the experimental data.

For a further test on the surface potential we plot in Fig. 3 experimental and theoretical rainbow angles, as a function of the perpendicular energy $E_{i\perp}$, for incidence along the $\langle 110 \rangle$ and $\langle 100 \rangle$ directions of LiF(001) [13]. For both channels the eikonal curves obtained by using the proposed atom–surface interaction follow closely the experimental results. As evident from Fig. 3(a), along the $\langle 110 \rangle$ direction eikonal rainbow angles are strongly affected by the projectile polarization, running below the experimental data at low electron energies ($E_{i\perp} \lesssim 1.5$ eV) when $V_{SP}^{(pol)}$ is neglected in the surface potential. But for larger $E_{i\perp}$ or for incidence along the $\langle 100 \rangle$ channel the influence of the polarization becomes small. The latter effect is a consequence of the ordering of the halide and alkali ions in the $\langle 100 \rangle$ channel, with opposite F^- and Li^+ asymptotic charges placed in front of each other, compensating their contributions to the polarization potential to order R^{-4}.

5. Conclusions

From the agreement between the experimentally observed angular positions of the supernumerary rainbows and the results from eikonal angular distributions, we conclude that a pairwise additive potential including polarization provides a reasonable approximation for the Ne–LiF interaction for perpendicular energies ranging from 0.07 to 5 eV. We also found that the projectile polarization is essential to describe the diffraction patterns for incidence along the $\langle 110 \rangle$ channel, while in the direction $\langle 100 \rangle$ its contribution is negligible.

Acknowledgments

M.S.G. and J.E.M. acknowledge financial support from CONICET, UBA, and ANPCyT of Argentina. This work was supported by the DFG under contract Wi 1336. The assistance of S. Wethekam and K. Maass in running the experiments is gratefully acknowledged. A.S. thanks the IMPRS-CS Ph.D. program of the MPG for financial support.

References

[1] A. Schüller, S. Wethekam, H. Winter, Phys. Rev. Lett. 98 (2007) 016103.
[2] P. Rousseau, H. Khemliche, A.G. Borisov, P. Roncin, Phys. Rev. Lett. 98 (2007) 016104.
[3] A. Schüller, H. Winter, Phys. Rev. Lett. 100 (2008) 097602.
[4] N. Bundaleski, H. Khemliche, P. Soulisse, P. Roncin, Phys. Rev. Lett. 101 (2008) 177601.
[5] M.S. Gravielle, J.E. Miraglia, Phys. Rev. A 78 (2008) 022901.
[6] F. Aigner, N. Simonović, B. Solleder, L. Wirtz, J. Burgdörfer, Phys. Rev. Lett. 101 (2008) 253201.
[7] A. Schüller, M. Busch, S. Wethekam, H. Winter, Phys. Rev. Lett. 102 (2009) 017602.
[8] M. Busch, A. Schüller, S. Wethekam, H. Winter, Surf. Sci. 603 (2009) L23.
[9] A. Schüller, H. Winter, Nucl. Instrum. Meth. Phys. Res. B 267 (2009) 628.
[10] M.S. Gravielle, J.E. Miraglia, Nucl. Instrum. Meth. Phys. Res. B 267 (2009) 610.
[11] H. Khemliche, P. Rousseau, P. Roncin, V.H. Etgens, F. Finocchi, Appl. Phys. Lett. 95 (2009) 151901.
[12] A. Schüller, M. Busch, J. Seifert, S. Wethekam, H. Winter, K. Gärtner, Phys. Rev. B 79 (2009) 235425.
[13] A. Schüller, K. Gärtner, H. Winter, Eur. Phys. Lett. 81 (2008) 37007.
[14] A.J. García, J.E. Miraglia, Phys. Rev. A 74 (2006) 012902.
[15] See Ref. [17] in Ref. [6].
[16] A. Schüller, H. Winter, M.S. Gravielle, J.M. Pruneda, J.E. Miraglia, Phys. Rev. A 80 (2009) 062903.
[17] H. Khemliche, N. Bundaleski, P. Soulisse, P. Roncin, Nucl. Instrum. Meth. Phys. Res. B 267 (2009) 620.
[18] A. Momeni, P. Soulisse, P. Rousseau, H. Khemliche, P. Roncin, e-J. Surf. Sci. Nanotechnol. 8 (2010) 101.
[19] J. Seifert, A. Schüller, H. Winter, R. Wlodarczyk, J. Sauer, M. Sierka, Phys. Rev. B 82 (2010) 035436.
[20] W.F. Avrin, R.P. Merrill, Surf. Sci. 311 (1994) 269.
[21] V. Celli, D. Eichenauer, A. Kaufhold, J.P. Toennies, J. Chem. Phys. 83 (1985) 2504.
[22] A.A. Abrahamson, Phys. Rev. 133 (1964) A990.
[23] Y.S. Kim, R.G. Gordon, J. Chem. Phys. 60 (1974) 4323.
[24] T.M. Miller, B. Bederson, D.R. Bates, B. Bederson, Advances in Atomic and Molecular Physics, vol. 13, Academic, New York, 1977, pp. 1–55.
[25] The used R_{0i} values are 1.24 and 1.76 a.u. for Li^+ and F^- target ions, respectively.
[26] F.W. Byron Jr., C.J. Joachain, Phys. Rev. A 9 (1974) 2559.
[27] M.V. Berry, K.E. Mount, Rep. Progr. Phys. 35 (1972) 315.
[28] C.J. Joachain, Quantum Collision Theory, North-Holland, Amsterdam, 1979.
[29] J.R. Manson, H. Khemliche, P. Roncin, Phys. Rev. B 78 (2008) 155408.
[30] The projectile distribution corresponding to $n_\perp = 1$ is smoothed in order to take into account the experimental broadening and scaled as $0.5 * P^{(eik)} + 0.05$, where the last term was introduced to include the inelastic background.